

Seasonality and Interannual Variations of Northern Hemisphere Temperature: Equator-to-Pole Gradient and Ocean–Land Contrast

SHALEEN JAIN AND UPMANU LALL

Utah Water Research Laboratory and Department of Civil and Environmental Engineering, Utah State University, Logan, Utah

MICHAEL E. MANN

Department of Geosciences, University of Massachusetts—Amherst, Amherst, Massachusetts

(Manuscript received 1 July 1997, in final form 20 April 1998)

ABSTRACT

Historical variations in the equator-to-pole surface temperature gradient (EPG) and the ocean–land surface temperature contrast (OLC) based on spatial finite differencing of gridded historical sea surface and land air temperatures are analyzed. The two temperature gradients represent zonally symmetric and asymmetric thermal forcings of the atmosphere. The strength and position of the Hadley cell and of the westerlies is related to the EPG, while the strength of the eddies coupled to the mid/high-latitude quasigeostrophic flow is related to the OLC. Taking these two parameters as simple yet highly meaningful diagnostics of the low-frequency variability of the atmosphere and climate system, the authors revisit a number of timely issues in the area of diagnostic climate studies. Of particular interest are seasonality and its variations and evidence of warming expected from greenhouse gas increases. Investigations of possible effects of CO₂-induced greenhouse warming are pursued by comparing the trends in EPG and OLC estimated from the observations and by using the Geophysical Fluid Dynamics Laboratory (GFDL) general circulation model (GCM) results for control and transient-increased CO₂ simulations. Significant differences are noted between the trends in EPG and OLC for observational data and the increased CO₂ GCM scenario. However, the dynamical response of both EPG and OLC during subperiods with warming and cooling is consistent with that exhibited by the GFDL GCM. In this sense, the “fingerprint” of anthropogenic forcing of the climate is not clearly evident in these basic diagnostics of large-scale climate variability.

1. Introduction

Much of the recent global warming debate has focused on an analysis of surface temperatures that exhibit an overall warming trend during this century (IPCC 1995; Jones et al. 1986). However, an analysis of surface temperature gradients may be more germane to a dynamical understanding of how the climate system may have changed over time. Two large-scale temperature gradients of particular interest are the (a) equator-to-pole temperature gradient (EPG) and (b) ocean–land temperature contrast (OLC). Changes in these temperature gradients have implications for meridional and zonal atmospheric circulation.

A latitudinally (i.e., zonally) symmetric equator-to-pole temperature gradient is important since (a) it is an important governor of poleward energy flux, the mean

potential energy [the main energy source for the circulation of the atmosphere (e.g., van Loon 1979; Peixoto and Oort 1992, 142, hereafter PO)], and the total eddy transport of sensible heat in winter; (b) it is a measure of baroclinicity, which determines the evolution of weather systems (PO, 142); (c) it is a surrogate for the strength of the extratropical height-averaged zonal flow through a thermal wind balance (PO, 156); and (d) it may strongly influence the position and strength of the tropical Hadley cell and the subtropical and subpolar high and low pressure belts, respectively, and hence the meridional water vapor transport. The EPG varies vertically and is steepest at the surface. However, the surface EPG corresponds to near-surface baroclinicity and correlates well with the strength of the upper-atmospheric zonal flow. Stone and Yao (1990) parameterize atmospheric poleward water vapor transport as proportional to EPG^{3.5} using a formula similar to that used for atmospheric sensible heat transport. Such transports are consequently very sensitive to the EPG. Lindzen (1994) argues that paleoclimate changes were associated with nearly unchanged equatorial temperatures and dramatic changes in the equator-to-pole (meridio-

Corresponding author address: Prof. Upmanu Lall, Utah Water Research Laboratory, Dept. of Civil and Environmental Engineering, Utah State University, Logan, UT 84322-8200.
E-mail: ulall@cc.usu.edu

nal) gradient and that the mean planetary temperature change may be best viewed as a residual arising from a change in the equator-to-pole temperature distribution. Tang and Weaver (1995) consider an interesting interplay between global temperature increase, a corresponding decrease in EPG, an atmospheric moisture flux that reflects a trade-off between decreasing sensible heat and increasing latent heat transport, and the thermohaline circulation. Their work shows that oscillatory dynamics of poleward moisture transport and the thermohaline circulation can change dramatically under climate warming. Connections between trends in regional winter temperatures and the circulation on the scale of long waves are demonstrated by van Loon and Williams (1976). In the context of our research, these works highlight the need to look at the trends in both the EPG and the average temperature as surrogates for sensible and latent heat transport to describe the state of the system.

The zonally asymmetric temperature gradient (OLC), which is linked to the longitudinal heating contrast between the ocean and the land, is important since (a) it is a measure of the principal thermal heterogeneity associated with an otherwise symmetrical circulation imparted by solar radiative forcing and the earth's rotation; (b) it is a determinant of the strength of the eddies coupled to the large-scale zonal flow (Lorenz 1984; Roebber 1995); (c) it plays a role in the amplification of eddies at the expense of the midlatitude zonal flow; and, hence, (d) it may be a measure of eddy water vapor transport and sensible heat fluxes (Stone and Yao 1990). Northern Hemisphere warming during the past century, for example, is associated with a high-latitude ocean-land temperature contrast pattern related to warming and subsequent cooling of the North Atlantic (e.g., Kushnir 1994; Mann and Park 1994, 1996b), which may have a dynamical source unrelated to radiative forcing (Delworth et al. 1993; Wallace and Renwick 1995; Wallace et al. 1996).

The structure, strength, and location of key features of the hemispheric circulation (e.g., the Hadley cell) are, in the simplified paradigm we adopt, determined by an interaction between the meridional temperature gradient (and its latitudinal variation), the latitude and strength of the heating center, and the strength of the eddies (related to the OLC). The seasonal variation in these factors translates into a variation in the strength, size, and location of the main meridional circulation cell—the tropical Hadley cell—and admittedly less statistically robust midlatitude and subpolar “Ferrel” cells, which arise from the the zonally averaged contribution of surface divergence in subtropical and subpolar high pressure belts and surface convergence in the region of the polar front. The interaction between the Hadley and Ferrel cells is considered as a possible conduit for interaction between subtropical and polar circulation, and may provide a mechanism for the chaotic generation of interannual and longer timescale variability throughout the climate system (e.g., Lorenz 1990). Consequently,

an analysis of the variations in the EPG and OLC provide a simple, idealized framework for the interpretation of low-frequency climate variability and, through their impact on circulation and moisture fluxes, provide the location and severity of extended droughts and floods. While the importance of these two interacting temperature gradients in determining circulation patterns has been recognized for some time [for instance, their use as key parameters in the highly simplified atmospheric circulation models of Lorenz (1984, 1990), Roebber (1995), Saltzman et al. (1989), and Wiin-Nielsen (1992)], there have been limited investigations of low-frequency variability in these diagnostic variables. Jain (1998) illustrates that modest changes in the mean EPG can lead to significant changes in the duration and character of seasons associated with the mean zonal flow and the superposed eddies represented in a low-order baroclinic model of Lorenz (1984, 1990). Jain (1998) also shows how the persistence and frequency of summer and winter atmospheric circulation regimes, their predictability, and degree of potential synchronization with tropical quasi-oscillatory phenomena are all sensitive to the EPG and OLC variation.

A goal of this paper is to provide a better understanding of the latitudinal structure, seasonality, and trends in the EPG and OLC over this century. The issues raised in Lindzen (1994) and Lindzen and Pan (1994) regarding the role of such gradients in modulating the tropical and midlatitude circulation at paleoclimatic timescales are arguably relevant to climatic changes in the last century as well. A question of interest is whether observed trends in the surface temperature gradients are consistent with expectations of greenhouse gas warming. The general climatology of the temperature gradients and their variation with latitude are studied. Interannual variability and the long-term trends in the EPG and OLC are also examined. These trends are compared to those expected from the Geophysical Fluid Dynamics Laboratory (GFDL) general circulation model (GCM) under a transient climate change scenario with CO_2 increasing at $1\% \text{ yr}^{-1}$ over a 100-yr period. To address questions of seasonality, observed changes in the amplitude and phase of the annual cycle in EPG and OLC are compared with the model's enhanced greenhouse scenario. A limited investigation of the latitudinal structure of the gradients follows.

2. Data

Three surface air temperature datasets (one observational and two from the GFDL GCM) are used in this study.

a. Northern Hemisphere temperature record

We use the gridded monthly time series of Northern Hemisphere (NH) surface temperatures prepared by the East Anglia group (see Jones et al. 1986; Jones and

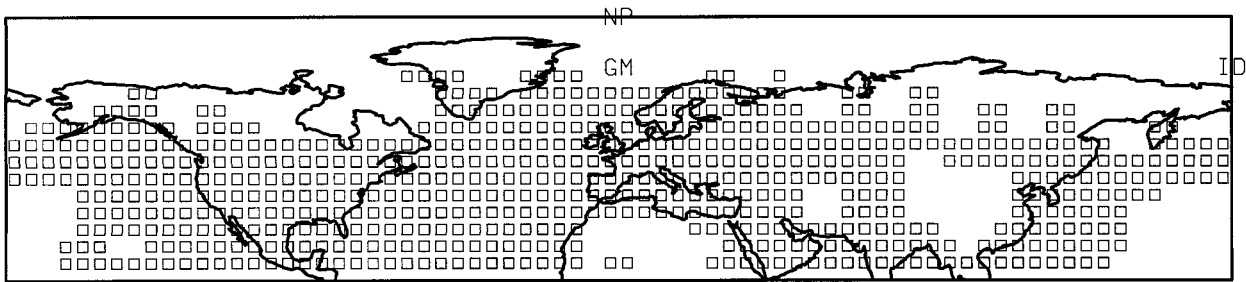


FIG. 1. Map showing the sampling grid of NH temperature data for the Jones–Briffa dataset used in the analysis. The GFDL sampling grid used was selected to conform closely to this grid.

Briffa 1992; Jones 1994), keeping only the subsample from 1898 to 1989 of grid points with nearly continuous monthly data as used by Mann and Park (1996a,b). A base period seasonal climatology was constructed during the 1950–79 period based on the average sea level temperatures for all of the contributing stations within a $5^\circ \times 5^\circ$ grid box (P. Jones 1997, personal communication). For land air temperature grid points, this requires that all stations be reduced to sea level before the calculations. There is some potential bias introduced due to the standard lapse rate assumption. However, spatial patterns of seasonality appear to be quite continuous and smooth at the larger-than-gridpoint scales (Mann and Park 1996a). The NH temperature data grid points are shown in Fig. 1. The monthly data for the period 1898–1989 is on a $5^\circ \times 5^\circ$ grid. The latitudinal coverage ranges from 15° to 75°N resulting in 12 latitude zones. Data for several grid points (e.g., East Asia and Pacific) are missing. Also, the data coverage for high latitudes ($>70^\circ\text{N}$) is minimal. Therefore, our analysis is based on the data in the 15° – 70°N latitudinal range. The analysis for the temperature and its gradients is expected to be somewhat biased due to the variable data coverage over land and ocean in a latitudinal zone. Some bias is also expected due to urbanization. Jones et al. (1989) have estimated that the overall effect of urbanization on temperature did not exceed 0.1°C over the past 100 years.

b. GFDL GCM data

GFDL GCM response to changing climate has been studied to gauge the possible effects of CO_2 -induced global warming (Manabe et al. 1991). Two simulations are available: one is a control run with CO_2 fixed, and the other is a transient run with equivalent CO_2 initialized at the 1958 amount and increased approximately 1% each year thereafter. Currently, the total CO_2 -equivalent radiative forcing due to various greenhouse gases other than water vapor is approximately $1\% \text{ yr}^{-1}$ (Manabe et al. 1991). Both runs are 100 yr long, with monthly data resolution. The grid resolution is 48×40 on a Gaussian grid. We have used model data in the 15° – 70°N latitudinal zones, corresponding to the observa-

tional data record and its spatial coverage to enable proper comparisons. Mann and Park (1996a) note, however, that the most significant changes in seasonality in response to increased CO_2 take place at polar latitudes. The sensitivity in the latitudinal range studied here might thus be expected to be smaller than in the excluded higher-latitude regions.

c. Derivation of EPG and OLC

The EPG and OLC time series are derived from the raw observed and model temperature data. The following datasets were developed: (a) monthly and annual zonal EPG, (b) monthly and annual zonal OLC, (c) monthly and annual hemispheric EPG, (d) monthly and annual hemispheric OLC, (e) annual hemispheric land and ocean temperature, and (f) annual hemispheric temperature.

Hemispherically averaged EPG and OLC series are used for the investigation of gross trends, while the zonally averaged time series are used to understand latitudinal structure of surface temperature gradients. The monthly time series are used to understand the seasonality of the fluxes and associated trends. The appendix provides details of the OLC and EPG computations. The zonal EPG time series is constructed using a weighted centered difference approximation. The weights reflect the areal extent of the various latitudinal zones. The resulting EPG consequently provides a better measure of the surface thermal energy gradient. Hemispheric EPG is computed as the slope of weighted regression between zonal temperature and latitude. Ocean–land contrasts are computed by taking the difference between the average land and ocean temperatures in a particular zone. Hemispheric OLC is computed as the difference between the average Northern Hemisphere land air and sea surface temperatures.

3. Major trends in the Northern Hemisphere temperature record

The temperature record is examined from the standpoint of (a) isolating the major trends and transitions, (b) identifying periods of warming and cooling whose

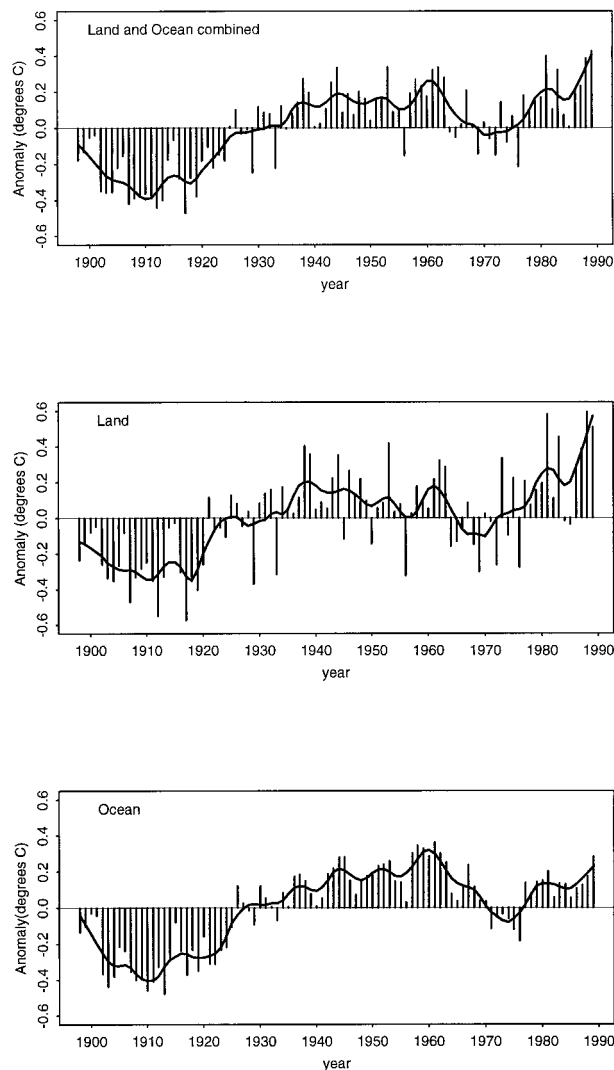


FIG. 2. The NH temperature record estimated from the Jones (1994) data. The smooth line in each panel represents a trend estimated using locally weighted regression (LOESS; see Cleveland and Devlin 1988) with a span of ~ 9 yr. Three periods are identifiable: 1898–1940 (warming), 1941–75 (cooling), and 1976–89 (warming).

attributes can be discussed later in a dynamical context, and (c) examining the difference in the response of land and oceans. We summarize previous findings in this regard to create a context in which the more complicated trends in OLC and EPG might be better understood.

The Northern Hemisphere temperature record has been studied extensively during the past decade (e.g., IPCC 1995; Jones et al. 1986; Jones and Briffa 1992). Land, ocean, and combined temperature series are shown in Fig. 2. The average temperatures show an overall increase in the present century. In the 1898–1989 record, a linear trend (significant at the 99% level) of $0.56^{\circ}\text{C} (100 \text{ yr})^{-1}$ is observed. Jones et al. (1986) reported that although there is an overall trend toward increase in the global temperature, the period between

the late 1930s and mid-1970s shows relatively steady conditions. Ghil and Vautard (1991) confirmed the flattening of the secular trend during the 1940–75 period. To be consistent with these studies, we identified three periods representing warming and cooling during 1898–1989: 1898–1940 (warming), 1941–75 (cooling), and 1976–89 (warming). Decadal variations in hemispheric temperatures are considered superimposed on top of these long-term trends. From Fig. 2, this classification appears appropriate for the land data. The combined land and ocean data show a cooling between 1898 and 1910, warming during 1910–40, little change between 1940 and 1960, cooling 1960–76, and warming thereafter. According to the analyses of Jones and Briffa (1992) the recent warming is largely an increase in winter land temperatures while summer periods are relatively unchanged. This can equivalently be viewed as a decrease in the amplitude of the annual cycle (Thomson 1995; Mann and Park 1996a). The correlation between ocean and combined ocean–land temperatures for 1976–89 drops to 0.33, while the land and combined temperature correlation increases to 0.97. The 1976–89 period has the weakest correlation (0.16) between land and ocean temperatures. These correlations reflect a rapid land warming and a much slower ocean response over the period.

The different timescales of evolution of land and ocean temperatures lead to variations in the ocean–land temperature contrast, which should translate into changes in atmospheric circulation patterns. A variety of empirical studies have isolated important interdecadal changes in sea surface temperatures in the North Atlantic (Kushnir 1994; Mann and Park 1994) and North Pacific (e.g., Trenberth and Hurrell 1994) and coupled variations in sea surface temperature and atmospheric circulation at those timescales (e.g., Trenberth 1990; Mann and Park 1996b). Coupled ocean–atmosphere modeling studies have produced similar signals in the Pacific (Latif and Barnett 1994) and Atlantic (Delworth et al. 1993). In both cases, significant perturbations in atmospheric circulation were noted. Wallace and Renwick (1995) find that nearly half the variance of monthly mean Northern Hemisphere (NH) temperature anomalies is linearly related to the amplitude of a cold ocean–warm land pattern north of 40°N , during warm periods. They argue that these patterns and the associated temperature trends have a dynamical origin and are unlikely to be the consequence of greenhouse gas–induced warming. Thus, substantial changes in OLC likely arise from dynamical changes in the climate that are unrelated to greenhouse warming. Other changes may relate to El Niño–Southern Oscillation (ENSO) and/or a greenhouse warming fingerprint (see, e.g., Trenberth and Hoar 1996). The roughly 50–70-yr timescale variability identified by Delworth et al. (1993) presumably impacts on the features we detect in the coupled ocean–atmosphere GFDL simulation.

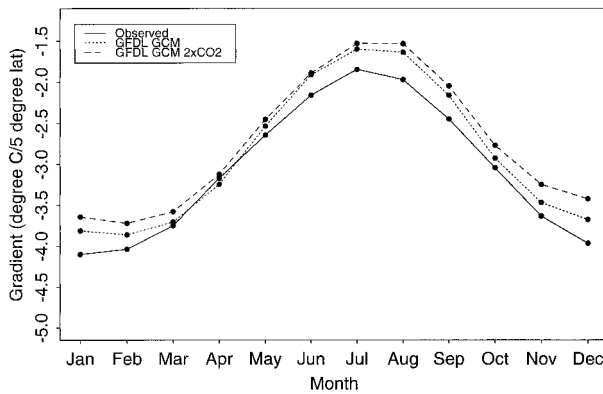


FIG. 3. The annual cycle of NH EPG for the Jones record and for the control and forced GCM runs.

4. General climatology of Northern Hemisphere EPG and OLC

The seasonal cycle of EPG and OLC is based on an average for each calendar month over the length of the data. The average climatology of the EPG and OLC exhibits a pronounced annual cycle (Figs. 3 and 4). The EPG is strongest during the winter months, since this is the period of maximum heating contrast between equator and pole. EPG weakens during the summers when the importance of mean meridional circulation for heat fluxes and kinetic energy is much smaller than during the winter (Palmén and Newton 1969).

The negative sign of the EPG values signifies the decrease in temperature with increasing latitude. The estimates from the observational record are qualitatively consistent with those reported in PO. However, the winter EPG values reported by PO are over $1^{\circ}\text{C} (5^{\circ}\text{lat})^{-1}$ higher than those obtained here. It is likely that some of these differences arise from the methodology (our finite differences are based on somewhat coarsely gridded data, so that gradients are likely to be smoothed out) while other differences relate to the variability of the climatology (our statistics are based on nearly a

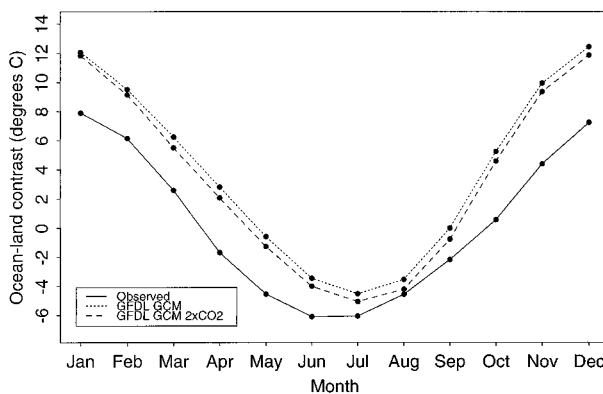


FIG. 4. The annual cycle of NH OLC for the Jones record and for the control and forced GCM runs.

TABLE 1. Seasonal and annual NH equator-to-pole gradients [$\text{in } ^{\circ}\text{C} (5^{\circ}\text{lat})^{-1}$].

	Annual	Summer (JJA)	Winter (DJF)
NH gridded data	-3.06	-1.99	-3.90
GFDL GCM forced	-2.74	-1.64	-3.59
GFDL GCM control	-2.87	-1.71	-3.77

century of data, while those of PO are based on a 30-yr climatology). The summer EPG distribution is in close agreement with the PO values.

A comparison between the seasonal cycle of EPG (see Table 1) for GFDL control and forced simulations shows a slight weakening of gradients under greenhouse warming and a reduction in the amplitude of the annual cycle of EPG. GFDL GCM control and forced EPG seasonal amplitudes are lower in magnitude than for the observed series, with weaker winter and summer gradients. The average annual EPG for the GFDL control simulation is slightly smaller than that for the observational record. The GCM simulations can consequently be expected to have weaker westerlies in the winter and a lower probability of organized zonal flows in the summer. Also, the annual cycle of monthly temperatures shows a broader range of temperatures for the GFDL model; the mean annual temperature for GFDL model is 10°C compared to the observed value of $\sim 15^{\circ}\text{C}$ for the range of latitudes considered here. It should be noted that flux corrections (see Manabe et al. 1991) have a strong influence on the model's seasonal cycle and may preclude meaningful quantitative comparisons between model and observed trends in seasonality.

The observed average annual OLC value is 0.32°C . OLC is a negative in the summer, as the average land temperatures exceed those over the oceans and vice versa during the winter (see Table 2). The minimum and maximum values for the OLC are -6° and 7.9°C , respectively. The GCM OLC values are very different from those in the observations. The average annual OLC is nearly 3.5°C higher for the control simulation and nearly 5°C higher in the winter. The eddy fluxes and other disturbances are consequently likely to be much more important in the GCM than in the climate system. GFDL GCM forced simulations exhibit a decrease in OLC during winters and an increase in the summer. However, these changes are small compared to the dif-

TABLE 2. Seasonal and annual NH ocean-land contrast ($\text{in } ^{\circ}\text{C}$).

	Annual	Summer (JJA)	Winter (DJF)
NH gridded data	0.32	-5.54	6.51
GFDL GCM forced	3.26	-4.41	10.92
GFDL GCM control	3.85	-3.80	11.42

Note: The values for the transient CO_2 -increased simulation are based on the time averages over the 60th- to 80th-yr period of the integration, to reflect the CO_2 doubling scenario.

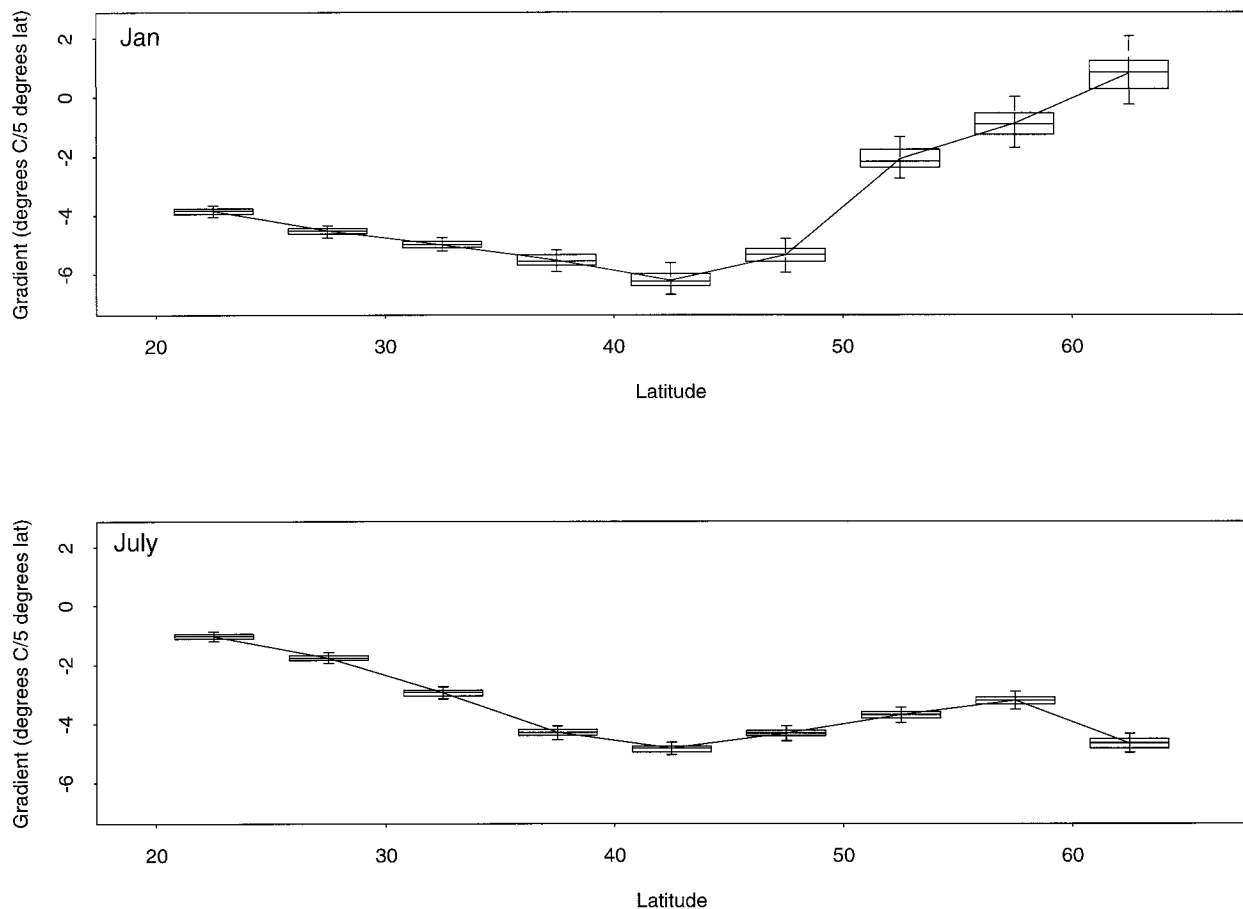


FIG. 5. Latitudinal profile of EPG corresponding to the seasonal extremes (Jan and Jul). The box plots show the variability in the EPG values across the years in the record. The extent of boxes corresponds to the 25th and 75th percentiles. The 50th percentile is shown by a line inside the box. The whiskers are extended to cover the 5th and 95th percentiles.

ference between the GCM and the observed values. A decrease in the winter OLC due to warming could correspond to a relatively larger increase in land temperatures than ocean temperatures. The warming between 1976 and 1989 showed such a pattern, in part for the reasons provided earlier.

The latitudinal structure of EPG exhibits seasonal variation (Fig. 5). The EPG increases northward, peaking in the 40°–45°N zone. In January, the gradients weaken toward the higher (>45°N) latitudes. The weakening in the EPG is related to the increased land fraction in these latitudes where landmasses are covered with snow and so meridional gradients diminish. Also, the oceanic component of meridional energy transport is negligible in these latitudes (Vonder Haar and Oort 1973). In July, the EPG declines between 40° and 60°N and then increases toward the poles, reflecting the heat flux toward the polar ice boundary. The annual EPG pattern is a combination of the winter and summer patterns. The summer EPG behavior appears to be dominated by the heat flux from the Tropics, which are nearly at a constant temperature, while the winter EPG behavior reflects a

polar influence. The variability in EPG is greatest in high latitudes in the winter and least in the Tropics. In winter, the 35°–45°N EPG is negatively correlated (monthly correlation ranging between -0.4 and -0.8) with the 55°–65°N EPG. All other correlations outside a 10°N latitude band around each latitude are small. In summer, the 25°–35°N EPG is negatively correlated (monthly correlation ranging between -0.4 and -0.6) with the midlatitude 45°–55°N. Once again, all other correlations outside a 10° latitude band are small. The seasonal differences may reflect the movement of the Hadley cell over the year and the associated energy fluxes.

Seasonal variations in the NH OLC by latitude are shown in Fig. 6. A poleward increase in OLC is observed in January. The almost linear increase in the OLC is caused by the relatively larger decrease in the land temperatures in the higher latitudes. The July OLCs are dominated by warmer temperatures over land. OLC attains a minima at the 47.5°N zone. This occurs due to the change in the distribution of radiative forcing and the increase in the land fraction as a function of latitude.

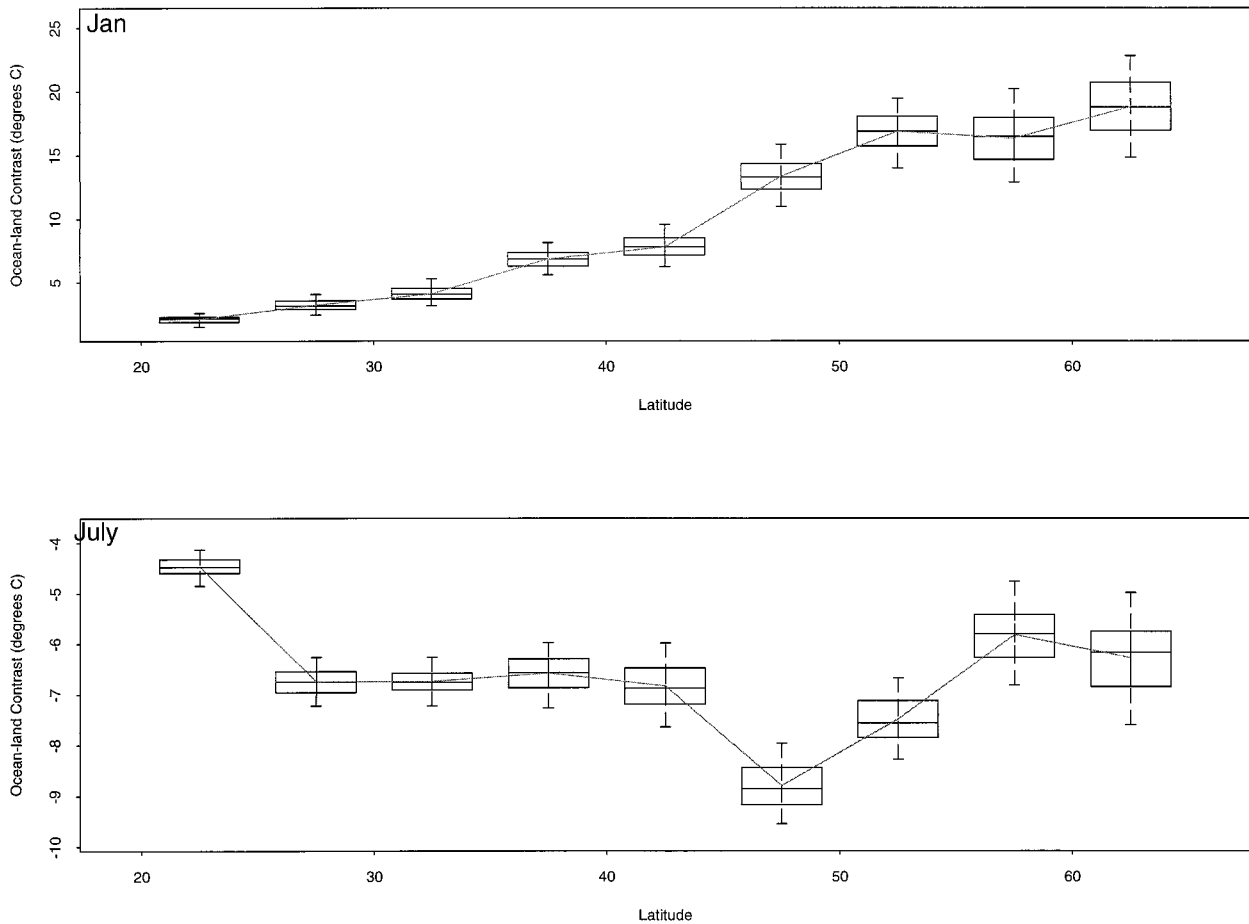


FIG. 6. Latitudinal profile of OLC corresponding to the seasonal extremes (Jan and Jul). The box plots show the variability in the EPG values across the years in the record. The extent of boxes corresponds to the 25th and 75th percentiles. The 50th percentile is shown as a line inside the box. The whiskers are extended to cover the 5th and 95th percentiles.

The variability in the OLC is least in the subtropics and maximum around 60°N. A higher-incident solar radiation in summer causes pronounced convective activity and vertical heat fluxes, predominantly over land. In the summer, a higher variability in the high-latitude OLC can be attributed to the significant changes in atmospheric circulation resulting from changes in the extent of snow cover in these latitudes and the weakening of the jet stream and polar fronts.

5. Trends in EPG and OLC

In this section, long-term trends in the surface temperature gradients are examined. Of particular interest are the time periods in which the temperature and associated gradient show consistent trends. We also compare the trends in the observed data with the results from the GFDL GCM simulations.

The January and July NH EPG and OLC time series for the GFDL GCM forced runs are shown in Fig. 7. The forced GCM run exhibits a monotonic increase in temperature over the record, a monotonic decrease in

OLC, and a monotonic decrease in the magnitude of EPG. The EPG weakens in the winter months while the summer gradients exhibit no clear trends with the CO₂-induced warming. The OLC trend is a homogenous decrease across the seasons corresponding to an apparent differential increase in the land temperatures.

The monthly time series for NH EPG and OLC were examined for significant trends during the full record and the three periods of warming and cooling (1898–1940, 1941–75, and 1976–89). Over the full period of record (1898–1989), there is no evidence of a monotonic trend in the historical EPG or OLC, while the Northern Hemisphere temperature series shows a monotonic increase. There is a small, statistically significant trend for a strengthening of the summer EPG (Table 3). This pattern is contrary to expectations from the CO₂-forced GCM run. The EPG time series show significant trends in the first two periods. During these periods, the ocean–land contrast time series shows no significant trend. However, during the 1976–89 period, no trend was detected in the EPG series, but the OLC shows a significant overall trend.

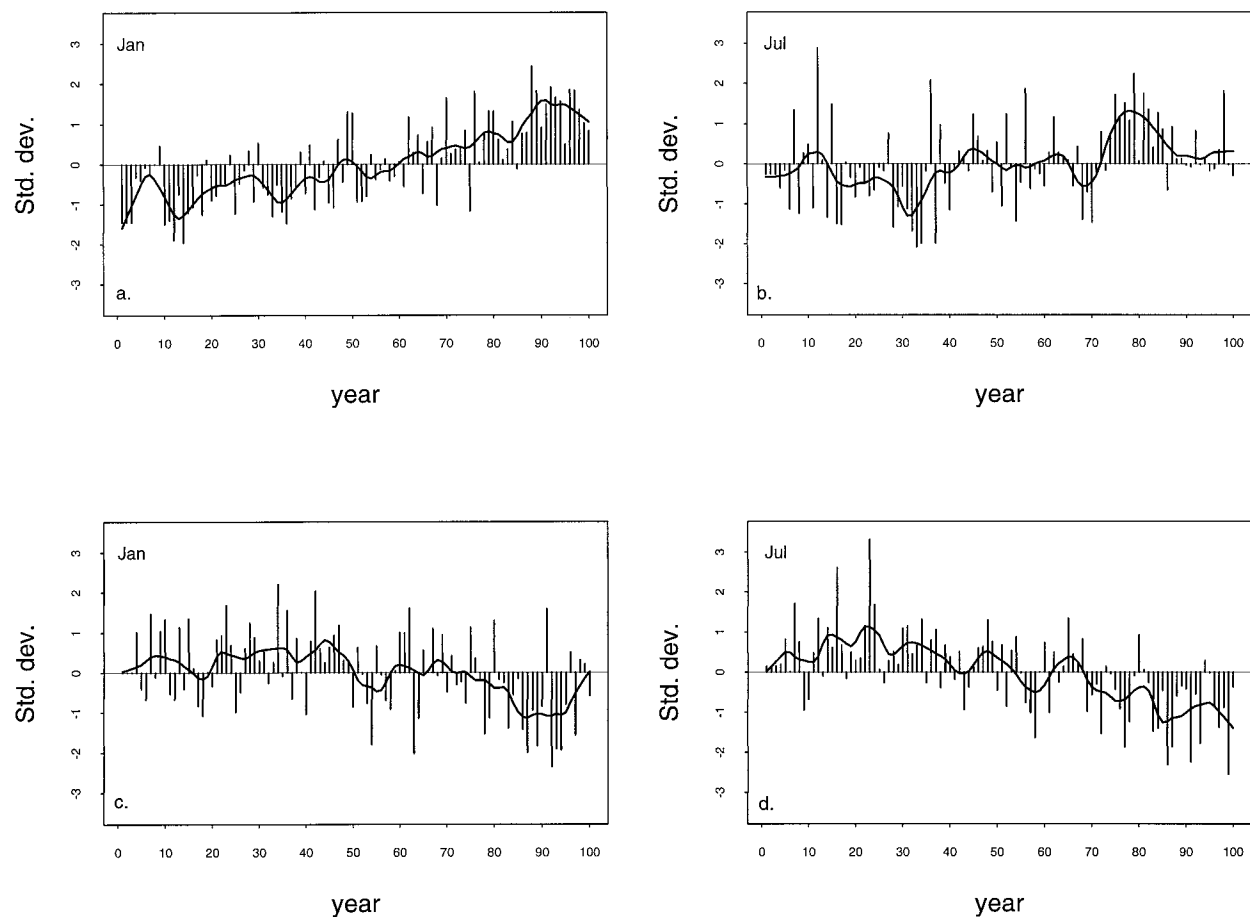


FIG. 7. Northern Hemisphere EPG and OLC time series for the GFDL GCM forced runs. (a) EPG for January, (b) EPG for July, (c) OLC for January, and (d) OLC for July. The standardized anomalies were computed using the mean and standard deviation for the full record for the target variable for the month in question.

The NH EPG and NH temperature anomalies are shown in Fig. 8. The warming in the 1898–1940 period corresponds to a weakening of EPG, consistent with expectations from the forced GCM run. The period between 1941 and 1975 was marked by a leveling off and a subsequent decrease in the NH combined land and ocean temperatures (ocean temperatures increase), with an associated increase (more negative) in EPG. During the 1976–89 period, the temperature increased, but no clear evidence of an EPG trend can be detected. Thus the analysis by subperiod suggests that the dynamics of the system response is not consistent with the forced

CO₂ GCM response, except perhaps for the first period. An analysis of seasonal EPG variations provides additional insight.

From Fig. 9, one observes that there is pronounced interdecadal variability in the summer and winter EPG but no clear evidence of a monotonic trend. Variability at these interdecadal-to-century timescales is probably related as much to previously described modes of natural oceanic and coupled ocean–atmosphere variability as to any anthropogenic influences. There is no clear phase correspondence (EPGs are anticorrelated up to 1925 and correlated from 1970) between the winter and summer

TABLE 3. Tests for significance in trends using the seasonal Mann–Kendall statistic and trends common to all months estimated using Sen's nonparametric slope estimator (Gilbert 1987).

Period	Equator-to-pole gradient (trend) in °C (5° lat) ⁻¹ yr ⁻¹	Uniform monthly trends?	Ocean–land contrast (trend) in °C yr ⁻¹	Uniform monthly trends?
1898–1940	Yes (+0.0019)	Yes	No	—
1941–75	Yes (−0.0012)	Yes	No	—
1976–89	No	—	Yes (−0.017)	Yes
1898–89	Summer (−0.0004)	No	No	—

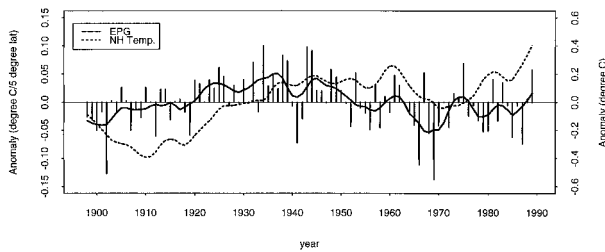


FIG. 8. Observed variations in the annual NH EPG and temperature for the 1898–1989 record. The vertical bars show the year-by-year variations in EPG, and the trend lines represent a smoothing of the EPG and the temperature series using LOESS with a span of 9 yr.

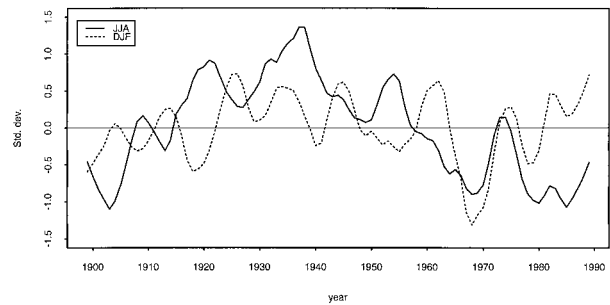


FIG. 9. Smoothed standardized anomalies of summer [Jun–Aug] and winter [Dec–Feb] EPG for the 1898–1989 record. The standardized anomalies were computed using the mean and standard deviation for the full record for the target variable for the season in question. They were smoothed using LOESS with a span of 9 yr.

series at these timescales. The summer trends for the two warming periods (1898–1940 and 1976–89) are opposite, while the winter trends are of the same sign, suggesting that this is unlikely to be the fingerprint of global warming as depicted by the GFDL GCM.

The standardized anomalies of the EPG for three zones (20° – 25° N, 40° – 45° N, 60° – 65° N) are shown in Fig. 10. During the 1898–1915 period, the EPG in the 20° – 25° N zone increased and then weakened by 1920. The EPG strengthened during 1920–40, then increased rapidly until 1945, and has generally strengthened since. The 40° – 45° N EPG shows a pronounced decadal pattern over the length of the record, with an increase in EPG between 1935 and 1955, and a general weakening thereafter. The 60° – 65° N latitudes show a rapid weakening of the EPG during the first decade of this century. Subsequently, the 60° – 65° N trend is either flat or shows an increase in EPG. These observations are contrary to expectations regarding global warming, where equatorial temperatures stay nearly constant, higher latitudes warm, and there is a general weakening of EPG at all latitudes. The slow timescale of ocean circulations and their interaction with the atmosphere may provide an explanation for the rich variety in the observational gradients response relative to the GFDL GCM.

OLC represents the dynamical variations in the quick land response and the delayed (and persistent) ocean response. In the 1900–20 period (see Fig. 11), the OLC exhibited persistent negative anomalies (relatively warmer land). Between 1920 and 1960 there was a general increase in the OLC, corresponding to a warmer ocean, while the temperature series also show an increasing trend. The OLC has decreased monotonically since 1970. One expects OLC to decrease under global warming scenarios. This happens only after 1965. Seasonal time series of the OLC (see Fig. 12) have similar trends. The latitudinal variations in the OLC are related to the ocean–land fraction in a latitude zone. From Fig. 13, one observes that the mid- and high latitudes show a recent decrease in OLC consistent with the observations of global warming. As generally expected under scenarios of warming, the low latitudes do not show much evidence of trends in OLC but are marked by pronounced interannual variability.

In summary, the last two decades exhibit trends in temperature and OLC that can be seen as broadly consistent with expectations from GCMs. This may suggest that we have a signal of global warming. Such a conclusion needs to be tempered by the lack of evidence of such a trend in the earlier period marked by a general global warming, by the pronounced interdecadal and interannual variability in the variables examined, and by the lack of decrease in EPG over this period. Further, while the temperature and EPG trends are consistent with forced GCM expectations in the earlier warming period (1898–1940), they are not accompanied by a confirmatory decrease in OLC. More work needs to be done in examining the response of high-resolution coupled models to a realistic combination of external forcings.

6. Trends in seasonality

Recent research has shown some evidence (Thomson 1995; Mann and Park 1996a) of shifts in the seasonal cycles of temperature in response to global warming trends. The changes in the amplitude and phase of the seasonal cycle are important for regional climate assessment. Changes in the phase may result due to century-scale natural variability of the climate system (e.g., Delworth et al. 1993; Kushnir 1994; Mann et al. 1994; Schlesinger and Ramankutty 1994) and the precession of equinoxes (Thomson 1995). Evidence has been provided for both greenhouse-related and solar-related influences on amplitude trends in the annual cycle (Thomson 1995; Mann and Park 1996a). We examine the changes in the phase and amplitude of the annual cycle of meridional temperature gradient and that of the ocean–land contrast over the length of the record.

Mann and Park (1996a) found a decrease in the amplitude of the annual cycle of NH temperature that is consistent with results from the forced GFDL GCM. The trend in phase for the models, however, is opposite to that observed and exhibits a delay, rather than an advance, of the seasons. The magnitude and the significance of the trends in the forced GFDL simulation di-

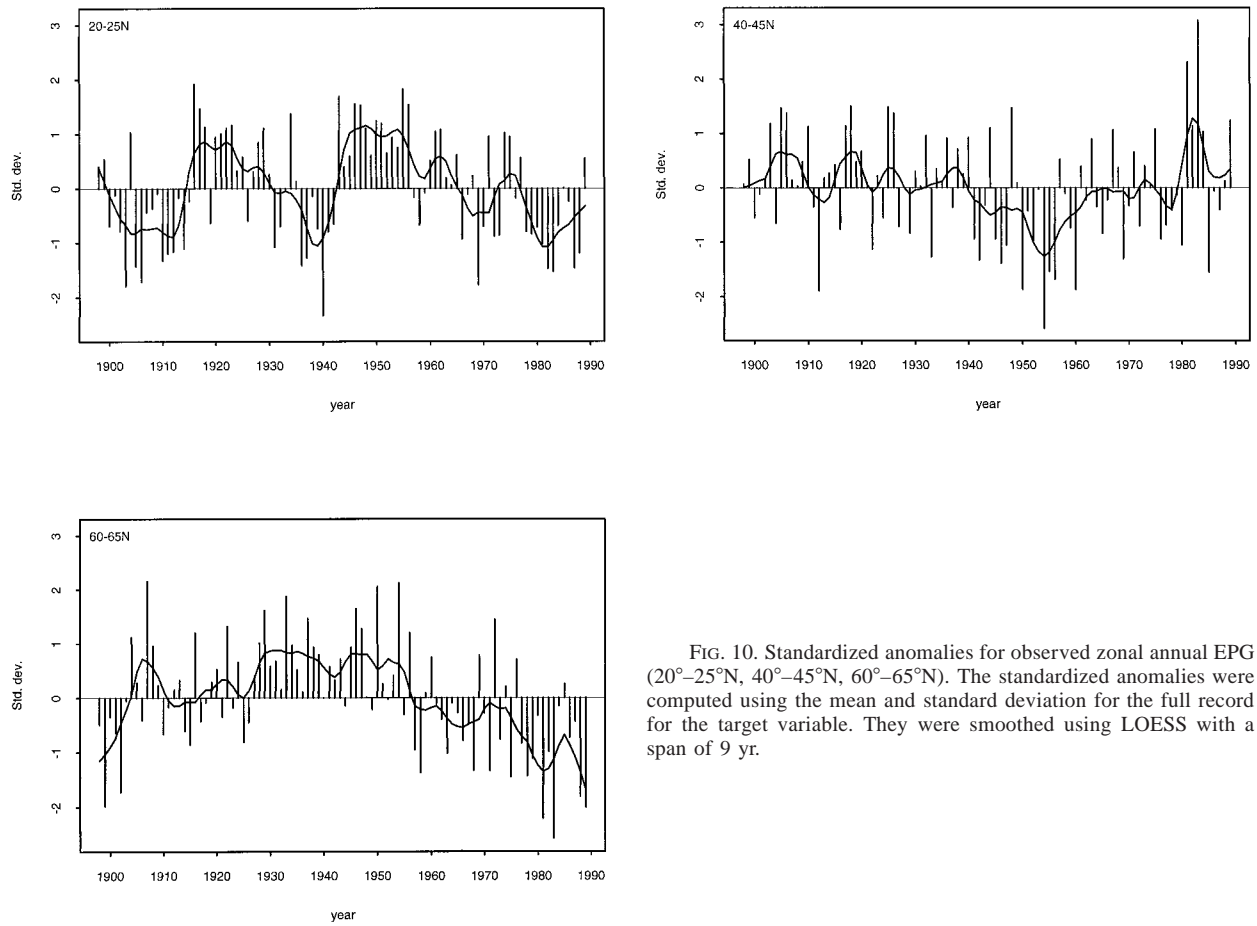


FIG. 10. Standardized anomalies for observed zonal annual EPG (20°–25°N, 40°–45°N, 60°–65°N). The standardized anomalies were computed using the mean and standard deviation for the full record for the target variable. They were smoothed using LOESS with a span of 9 yr.

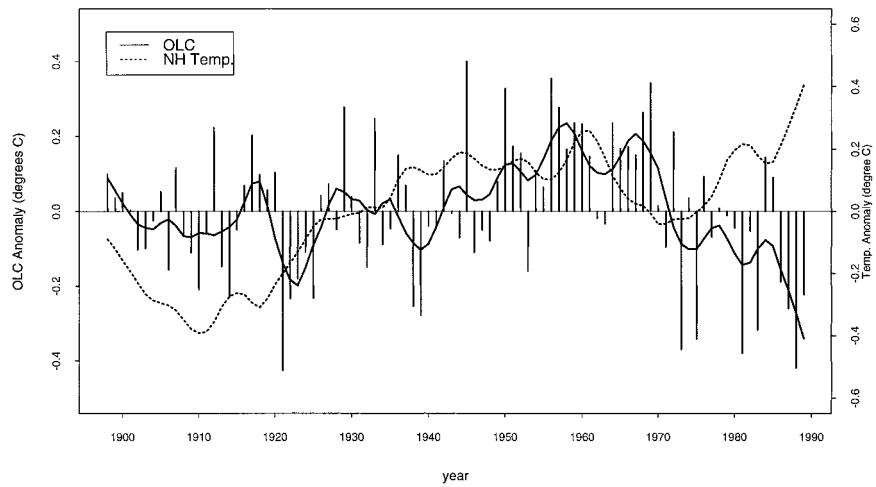


FIG. 11. Observed variations in the annual NH OLC and temperature for the 1898–1989 record. The vertical bars show the year-by-year variations in OLC, and the trend lines represent a smoothing of the OLC and the temperature series using LOESS with a span of 9 yr.

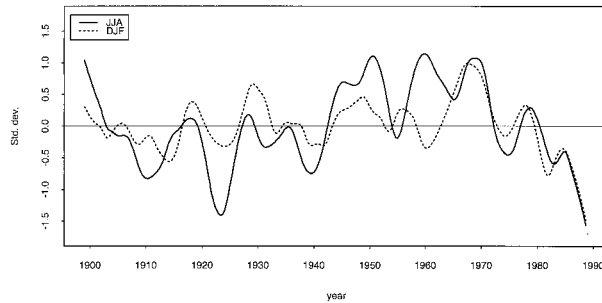


FIG. 12. Smoothed standardized anomalies of standard deviation of summer (JJA) and winter (DJF) OLC for the 1898–1989 record. The standardized anomalies were computed using the mean and standard deviation for the full record for the target variable for the season in question. They were smoothed using LOESS with a span of 9 yr.

minish if high- and low-latitude regions, poorly sampled by the observational data, are excluded, but no latitude band exhibits the phase advance found in the observations. The control GFDL simulation, like the observations, exhibits a marginally significant advance in phase, perhaps associated with organized century-scale variability.

The methodology used to analyze the temperature

gradients is that of Mann and Park (1996a) and is based on a multivariate generalization of multitaper complex demodulation (see Thomson 1982; Park 1992). The seasonal cycle of temperature gradients is approximated as $A(t) \cos[2\pi t + \varphi(t)]$, where t is in years, and $A(t)$ and $\varphi(t)$ are the amplitude and phase associated with the fundamental mode of seasonal variations, respectively. A time frequency bandwidth product $p = 2$ and $K = 3$ Slepian tapers with a 10-yr moving window to estimate $A(t)$ and $\varphi(t)$ using complex demodulation. Linear trends are fit to the $A(t)$ and $\varphi(t)$ estimated from the frequency domain analysis (see Fig. 14). We test for statistically significant trends of phase corresponding to an advance or delay of seasons against a null hypothesis for no trend. The temperature data show a switch in the trends around 1940. Hence we have estimated the phase and amplitude trends for the pre-1940 and post-1940 years separately. Results of these analyses are summarized in Table 4.

From the analysis of the forced GFDL GCM data, we expect a statistically significant advance of about 4 days over 100 yr in the seasonal cycle of EPG, with an attendant decrease in amplitude of about 0.13°C . A statistically significant delay in phase and increase of am-

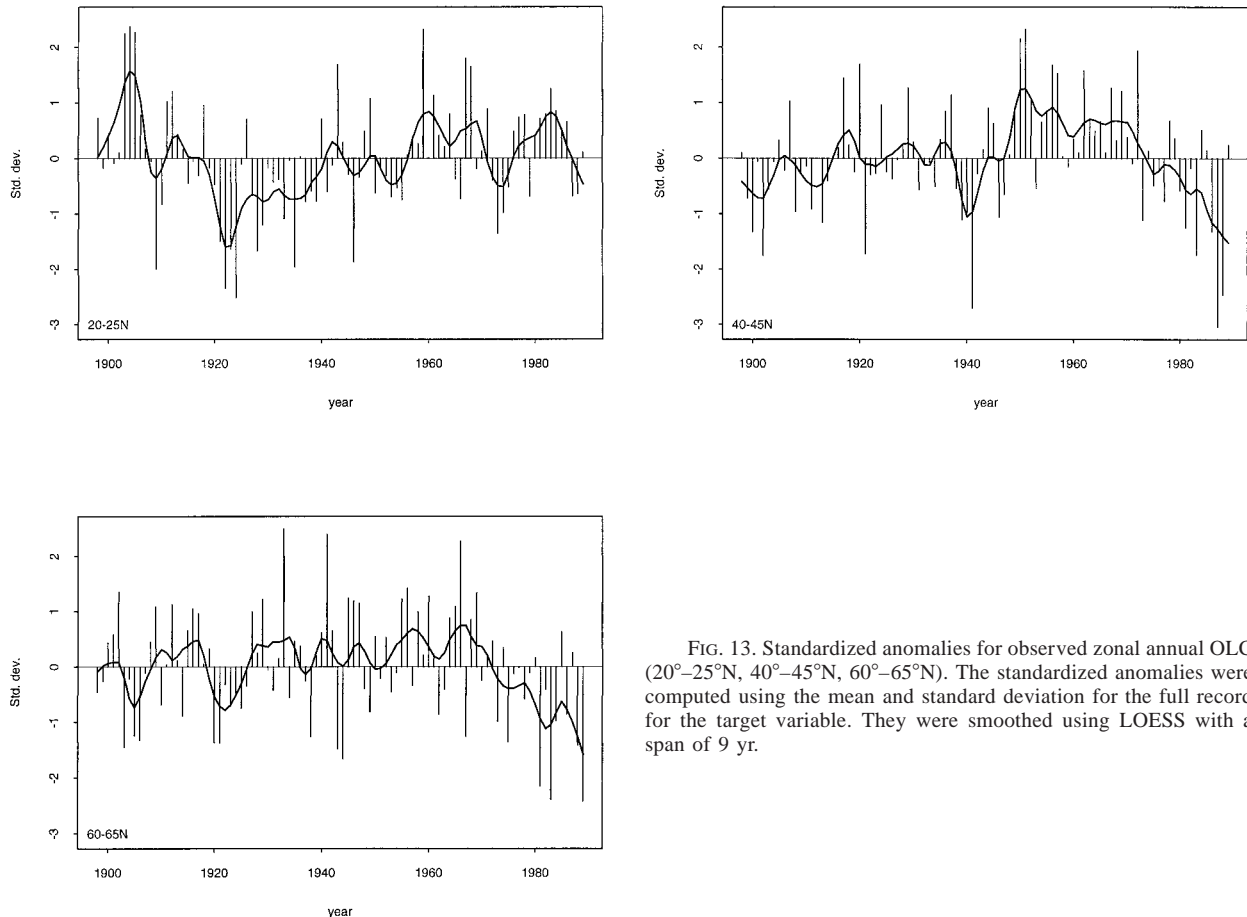


FIG. 13. Standardized anomalies for observed zonal annual OLC (20° – 25°N , 40° – 45°N , 60° – 65°N). The standardized anomalies were computed using the mean and standard deviation for the full record for the target variable. They were smoothed using LOESS with a span of 9 yr.

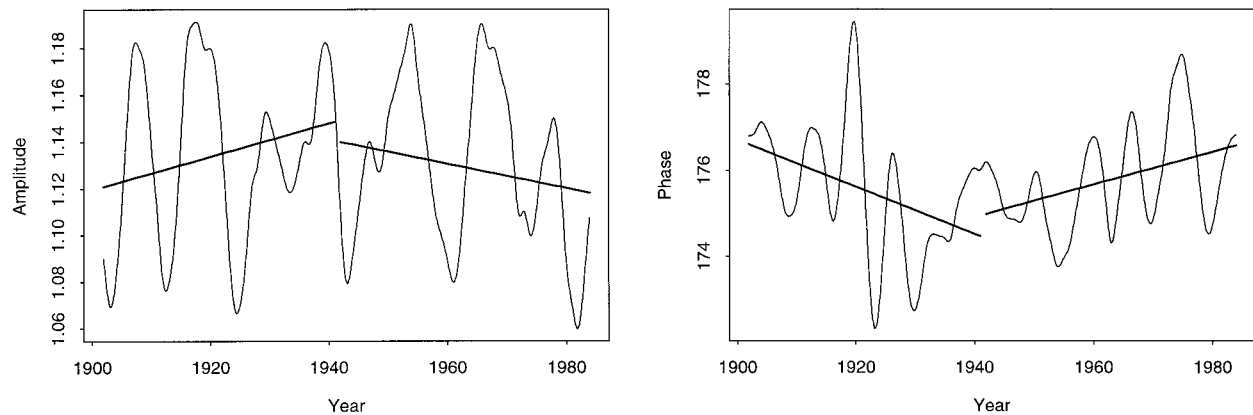


FIG. 14. Trends in the (a) amplitude and (b) phase of the annual cycle of the NH EPG. The amplitude and phase were computed using a moving window of 10 yr centered on the target year. Trend lines for the pre- and post-1940 periods are also shown in each case. The interdecadal variations are markedly stronger than the underlying longer-period trends.

plitude in OLC's annual cycle is also observed. However, even the control GFDL run shows a statistically significant increase in amplitude of OLC over the 100-yr run, suggesting the effect of either model drift or enhanced century-scale variability.

The EPG for the 1898–1989 record does not show a significant trend in either the phase or the amplitude of the annual cycle (see Fig. 14). Indeed, the sign of the changes is opposite to those expected from the forced GCM run. The 1900–1940 warming subperiod shows a statistically significant advance in the phase of the EPG cycle of about 5 days $(100 \text{ yr})^{-1}$ but shows no trend in the amplitude. The 1941–83 period has a statistically significant delay in phase of about 4 days $(100 \text{ yr})^{-1}$. A closer look at Fig. 14 suggests an oscillatory behavior in the phase and amplitude for NH EPG. This decadal variation in phase is rather interesting. Such a behavior

may be associated with slowly varying forcing provided by the oceans. Since the NH temperature is generally decreasing over this period, the responses over the two periods are dynamically consistent with those expected from the GCM. However, the overall trend is clearly not a GCM greenhouse warming signature. The OLC exhibits a statistically significant trend in phase [delay of about 3 days $(100 \text{ yr})^{-1}$] for the full record. No other trends are significant. This trend is determined largely by anomalous events in the last decade.

In summary, there is evidence of persistent interdecadal- or centennial-scale fluctuations in the phase but not the amplitude of the annual cycle in the temperature gradients for the pre- and post-1940 periods. Little evidence exists for secular trends in the phase and amplitude of the annual cycle of these gradients that match those indicated by the GFDL GCM. The changes in phase are only of the order of a few days per hundred years and would appear to be due at least in part to natural variability at interdecadal-to-century timescales.

TABLE 4. Fitted linear trends and the significance levels for the amplitude and phase of the annual cycles of NH EPG and OLC.

	$\Delta\phi$ (°)	<i>p</i> value	ΔA	<i>p</i> value
NH EPG				
Overall	0.29	0.57	0.01	0.57
1900–40	–2.19	0.01	0.02	0.17
1941–83	1.63	0.01	–0.02	0.24
NH OLC				
Overall	1.25	0.00	0.00	0.92
1900–40	–0.01	0.98	0.05	0.33
1941–83	0.01	0.56	–0.06	0.24
GFDL GCM 1% increase in CO ₂ (100-yr duration)				
EPG	–4.26	0.00	–0.13	0.00
LOC	0.90	0.01	0.12	0.03
GFDL GCM controlled CO ₂				
EPG	–0.09	0.83	0.00	0.92
LOC	0.18	0.66	0.24	0.00

Note: $\Delta\phi$ and ΔA are the total change in the phase and amplitude, respectively, over the specified period of time; the *p* value reported is for the significance level for a *t* test for the slope of a linear trend.

7. Summary

This paper was motivated by the observation that the equator-to-pole temperature gradient and the ocean–land temperature contrast of surface temperature may be useful measures of potential energy, moisture fluxes, and the strength and nature of the larger-scale circulation. Consequently, analyses of trends in these variables may complement interpretations of global change from analyses of temperature records. Indeed, these measures may be rather useful for fingerprinting global change as observed by Lindzen (1994). By the same token, they are useful diagnostics for GCMs.

An empirical investigation into the climatological behavior of and trends in the Northern Hemisphere meridional temperature gradient and ocean–land contrast was conducted based on nearly 100 yr of gridded surface

temperature data. The following key observations are made from this analysis.

- 1) Historical trends in the mean, decadal, and interdecadal variability, and seasonality of EPG and OLC seem to result from decadal-to-century-scale internal climate processes. The mechanisms may be related to modes of oceanic or coupled ocean–atmosphere variability that have been detected in observational data and isolated in recent coupled model simulation studies. A formal investigation of these issues using coupled ocean–atmosphere models will be of interest. Given the disparity in the characteristic time-scales for ocean and landmasses, it may be useful to extend the analysis of meridional gradients variations on land and oceans separately. Likewise, a separate analysis of the OLC for the Atlantic and the Pacific sectors may be insightful.
- 2) Consistent biases exist between observational and model estimates of the OLC and the EPG. These biases are manifested in the amplitude of the annual cycle, as well as the annual mean, and are especially large for the OLC. These biases probably result, at least in part, from seasonally specific gridpoint flux corrections imposed during model integrations.
- 3) The trends in mean NH temperatures, EPG, and OLC and the seasonality of these variables over the last century are not consistent with those projected for greenhouse warming by the GFDL coupled ocean–atmosphere enhanced CO₂ simulation. However, the dynamical response of the EPG and the OLC to periods of hemispheric warming and cooling is somewhat similar to what is observed in both control and enhanced greenhouse scenario simulations. In this sense, the characteristics of the dynamical relationship between variations in EPG and OLC is consistent between model and observation. Furthermore, a clear “fingerprint” of anthropogenic warming is not evident in these diagnostics based on the model–observational comparison. This lack of agreement probably arises from the significant impact of low-frequency natural variability, model flux corrections, and sampling limitations in the observational data. Model–data intercomparisons based on newer-generation coupled models may help to clarify the sources of these discrepancies.

Acknowledgments. The work presented here was supported in part by the National Science Foundation under Grant EAR-9720134. We would like to thank an anonymous reviewer for his/her constructive comments that led to a substantial improvement in the quality of this paper.

APPENDIX

Derivation of EPG and OLC Time Series

The EPG and OLC time series are derived from the surface air temperature data. Monthly temperature is represented as \bar{T}_{it} ,

$$\bar{T}_{it} = \sum_{j=1}^n \frac{T_{ijt}}{n}, \quad (\text{A1})$$

where $\overline{(\cdot)}$ represents the zonal average, $j = 1, \dots, n$ is the longitude index, i is the latitudinal zone index and $i = 1, \dots, m$, where m is the number of latitude zones, and t is a calendar month index and $t = 1, \dots, 12$; w_i represents a normalized weight associated with the latitudinal zone, such that

$$w_i = \frac{\cos(\phi_i)}{\sum_{i=1}^m \cos(\phi_i)}, \quad (\text{A2})$$

where ϕ_i is the latitude.

a. Monthly and annual zonal EPG

The monthly zonal EPGs are computed using a weighted centered difference approximation about the latitude of interest. The average zonal temperature may be somewhat biased due to lack of coverage in some latitudes:

$$\text{EPG}_{it} = \left(\frac{w_{i+1}\bar{T}_{t,i+1} - w_i\bar{T}_{t,i}}{w_{i+1} + w_i} + \frac{w_i\bar{T}_{t,i} - w_{i-1}\bar{T}_{t,i-1}}{w_i + w_{i-1}} \right), \quad (\text{A3})$$

where the annual average zonal EPG is computed as the average of monthly zonal EPGs:

$$\text{EPG}_i = \frac{1}{12} \sum_{t=1}^{12} \text{EPG}_{it}. \quad (\text{A4})$$

The EPG thus obtained is expressed in °C (5° lat)⁻¹.

b. Monthly and annual zonal OLC

The monthly and annual zonal ocean–land contrast is computed by taking the difference between the average ocean and land temperature in a latitudinal zone. Monthly zonal OLC is

$$\text{OLC}_{it} = \bar{T}_{it}^0 - \bar{T}_{it}^1, \quad (\text{A5})$$

where the superscripts 0 and 1 represent ocean and land, respectively.

Annual zonal OLC is

$$\text{OLC}_i = \frac{1}{12} \sum_{t=1}^{12} \text{OLC}_{it}. \quad (\text{A6})$$

c. Monthly and annual hemispheric EPG

The monthly average hemispheric EPG is obtained by solving the weighted least squares regression problem for the slope of the zonal temperature (\bar{T}) with respect to latitude (ϕ). Hence,

$$\text{EPG}_t = \frac{\sum_{i=1}^m w_i (\phi_i - \bar{\phi}') (\bar{T}_{it} - \bar{T}'_t)}{\sum_{i=1}^m w_i (\phi_i - \bar{\phi}')^2}, \quad (\text{A7})$$

in which

$$\bar{\phi}' = \frac{\sum_{i=1}^m w_i \phi_i}{\sum_{i=1}^m w_i} \quad (\text{A8})$$

and

$$\bar{T}'_t = \frac{\sum_{i=1}^m w_i \bar{T}_{it}}{\sum_{i=1}^m w_i}. \quad (\text{A9})$$

The annual NH EPG value is computed by averaging the monthly values.

d. Monthly and annual hemispheric OLC

The monthly hemispheric OLC is computed from the weighted average of the zonal OLCs,

$$\text{OLC}_i = \frac{1}{12} \sum_{t=1}^{12} \text{OLC}_{it}. \quad (\text{A10})$$

The annual series is computed as an average of the monthly NH OLC values,

$$\text{NHOLC} = \frac{1}{12} \sum_{t=1}^{12} \text{NHOLC}_t. \quad (\text{A11})$$

e. Annual hemispheric land and ocean temperature

The annual hemispheric land and ocean temperatures are computed by computing a weighted average across the respective average monthly zonal values.

f. Annual hemispheric temperature

The annual hemispheric temperature is computed from the zonal average temperature time series. A weighted average across the zonal time series yields the representative hemispheric temperature.

REFERENCES

- Cleveland, W. S., and S. J. Devlin, 1988: Locally weighted regression: An approach to regression analysis by local fitting. *J. Amer. Stat. Assoc.*, **83**, 596–610.
- Delworth, T., S. Manabe, and R. J. Stouffer, 1993: Interdecadal variations of the thermohaline circulation in a coupled ocean–atmosphere model. *J. Climate*, **6**, 1993–2011.
- Ghil, M., and R. Vautard, 1991: Interdecadal oscillations and the warming trend in global temperature time series. *Nature*, **350**, 324–327.
- Gilbert, R. O., 1987: *Statistical Methods for Environmental Pollution Monitoring*. Van Nostrand Reinhold, 320 pp.
- IPCC, 1995: *Climate Change 1995: The Science of Climate Change*. Cambridge University Press, 572 pp.
- Jain, S., 1998: Low-frequency climate variability: Inferences from simple models. M.S. thesis, Dept. of Civil and Environmental Engineering, Utah State University, 187 pp.
- Jones, P. D., 1994: Hemispheric surface temperature variations: A reanalysis and an update to 1993. *J. Climate*, **7**, 1794–1802.
- , and K. R. Briffa, 1992: Global surface air temperature variations during the 20th century, 1. Spatial, temporal, and seasonal details. *Holocene*, **1**, 165–179.
- , T. M. L. Wigley, and P. B. Wright, 1986: Global temperature variations, 1861–1984. *Nature*, **322**, 430–434.
- , P. M. Kelly, G. B. Goodess, and T. R. Karl, 1989: The effect of urban warming on the Northern Hemisphere temperature average. *J. Climate*, **2**, 285–290.
- Kushnir, Y., 1994: Interdecadal variations in North Atlantic sea surface temperature and associated atmospheric conditions. *J. Climate*, **7**, 141–157.
- Latif, M., and T. P. Barnett, 1994: Causes of decadal climate variability over the North Pacific and North America. *Science*, **266**, 634–637.
- Lindzen, R. S., 1994: Climate dynamics and global change. *Annu. Rev. Fluid Mech.*, **26**, 353–378.
- , and W. Pan, 1994: A note on orbital control of equator–pole fluxes. *Climate Dyn.*, **10**, 49–57.
- Lorenz, E. N., 1984: Irregularity: A fundamental property of the atmosphere. *Tellus*, **36A**, 98–110.
- , 1990: Can chaos and intransitivity lead to interannual variability? *Tellus*, **42A**, 378–389.
- Manabe, S., R. J. Stouffer, M. J. Spelman, and K. Bryan, 1991: Transient response of a coupled ocean–atmosphere model to gradual changes of atmospheric CO₂. Part I: Annual mean response. *J. Climate*, **4**, 785–818.
- Mann, M. E., and J. Park, 1994: Global-scale modes of surface temperature variability on interannual to century timescales. *J. Geophys. Res.*, **99**, 25 819–25 833.
- , and —, 1996a: Greenhouse warming and changes in the seasonal cycle of temperature: Model versus observations. *Geophys. Res. Lett.*, **23**, 1111–1114.
- , and —, 1996b: Joint spatio-temporal modes of surface temperature and sea level pressure variability in the Northern Hemisphere during the last century. *J. Climate*, **9**, 2137–2162.
- Palmén, E., and C. W. Newton, 1969: *Atmospheric Circulation Systems: Their Structure and Physical Interpretation*. Academic Press, 603 pp.
- Park, J., 1992: Envelope estimation for quasi-periodic geophysical signals in noise: A multitaper approach. *Statistics in the Environmental and Earth Sciences*, A. T. Walden and P. Guttorp, Eds., Halsted Press, 189–219.
- Peixoto, J. P., and A. H. Oort, 1992: *Physics of Climate*. American Institute of Physics, 520 pp.
- Roebber, P. J., 1995: Climate variability in a low-order coupled atmosphere–ocean model. *Tellus*, **47A**, 473–494.
- Saltzman, B., C.-M. Tung, and K. A. Maasch, 1989: Folded resonance and seasonal vacillation in a thermally-forced baroclinic wave model. *Atmosfera*, **2**, 131–154.
- Schlesinger, M. E., and N. Ramankutty, 1994: An oscillation in the global climate system of period 65–70 years. *Nature*, **367**, 723–726.
- Stone, P. H., and M. S. Yao, 1990: Development of a two-dimensional zonally averaged statistical-dynamical model. Part III: The parameterization of eddy fluxes of heat and moisture. *J. Climate*, **3**, 726–740.
- Tang, B., and A. J. Weaver, 1995: Climate stability as deduced from an idealized coupled atmosphere–ocean model. *Climate Dyn.*, **11**, 141–150.
- Thomson, D. J., 1982: Spectrum estimation and harmonic analysis. *Proc. IEEE*, **70**, 1055–1096.

- , 1995: The seasons, global temperature, precession, and CO₂. *Science*, **268**, 59–68.
- Trenberth, K. E., 1990: Recent observed interdecadal climate changes in the Northern Hemisphere. *Bull. Amer. Meteor. Soc.*, **71**, 988–993.
- , and J. Hurrell, 1994: Decadal atmosphere–ocean variations in the Pacific. *Climate Dyn.*, **9**, 303–319.
- , and T. J. Hoar, 1996: The 1990–1995 El Niño–Southern Oscillation event: Longest on record. *Geophys. Res. Lett.*, **23**, 57–60.
- van Loon, H., 1979: The association between latitudinal temperature gradient and eddy transport. Part I: Transport of sensible heat in winter. *Mon. Wea. Rev.*, **107**, 525–534.
- , and J. Williams, 1976: The connection between trends of mean temperature and circulation at the surface: Part I. Winter. *Mon. Wea. Rev.*, **104**, 365–380.
- Vonder Haar, T. H., and A. H. Oort, 1973: New estimates of annual poleward energy transport by Northern Hemisphere oceans. *J. Phys. Oceanogr.*, **3**, 169–172.
- Wallace, J. M., and J. A. Renwick, 1995: Dynamical contribution to hemispheric temperature trends. *Science*, **270**, 780–783.
- , Y. Zhang, and L. Bajuk, 1996: Interpretation of interdecadal trends in Northern Hemisphere surface air temperature. *J. Climate*, **9**, 249–259.
- Wiin-Nielsen, A., 1992: Comparisons of low-order atmospheric dynamic systems. *Atmosfera*, **5**, 135–155.